Effect of Noble Gas van der Waals Induced Dipoles on the Work Function of Metals†

Bruno Linder* and Robert A. Kromhout‡

Chemical Physics Program, The Florida State University, Tallahassee, Florida 32306-4390

Received: July 25, 2002

We derive the van der Waals induced moment using a reaction field approach based on charge density susceptibilities of several bodies interacting through Coulomb operators. We extend previous results to include nonadditive contributions from up to four bodies. We then expand the Coulomb operators in a moment T-tensor series. The lowest hyperpolarizability terms yielding nonzero values are products of the dipole−dipole quadrupole hyperpolarizability, *B*, for the body whose dipole moment is being evaluated and the dipole−dipole polarizabilities, α, of the other interacting bodies. We then introduce the image approximation for the case where one body is a solid and apply our results to the cases of argon and xenon on magnesium and on palladium. By closure, we are able to separate the frequency dependencies of the various factors so that this contribution can be reduced to a numerical factor that is then calculated by numerical integration. Our present results show that the work function reductions of magnesium by argon and xenon can be accounted for by our calculations. Our calculated reductions for palladium suggest that in the high work-function metals another mechanism enters in an important way, as has been suggested by others. The relationship between our present results and earlier estimates by ourselves and others is discussed.

I. Introduction

When two dissimilar systems interact, they give rise to a static moment. This is true even if the systems are spherical and even if they do not overlap. These moments manifest themselves in collision-induced spectroscopy, in the far-infrared and microwave spectroscopy of van der Waals complexes and of adsorbed molecules, and in the changes in the work function of metals in the presence of adsorbed molecular monolayers.[1,2]

In our 1986 paper,[3] we presented a systematic approach for obtaining the induced dipole of an arbitrary system interacting via the Coulomb potential with another arbitrary system. Dispersion, induction, and charge interpenetration effects were included, but exchange was neglected. These results were expressed in terms of charge-density susceptibilities and the full (unexpanded) Coulomb potential. Hunt[4] developed a related approach based on polarization density and the dipole propagator that for uncharged species can be shown to be equivalent and has successfully applied it to calculations of collision-induced spectra. By use of the image approximation, we specialized our results to the interaction of an atom and a nonferroelectric solid.[3]

In 1986, there were no available values for the atomic dipole−dipole−quadrupole hyperpolarizibility *B*, which was needed for the leading term in the calculation of the van der Waals moment of adsorbed atoms, but approximate calculations for argon, krypton, and xenon on palladium had yielded results that were much too small to explain the large (on the order of 1 V) reduction observed experimentally.[2b] More recent experimental[5] and theoretical[6] work has indicated that the neglect of mixing of excited atomic states with empty metal conduction states may be the problem when the Fermi level of the metal lies below the excited atomic levels that are important contributors in perturbation treatments of the dipole moment, and indeed the moments increase sharply as a function of the metal work function in the cases where the work function exceeds the excited-state ionization energy.[5] These considerations, together with the availability of values of *B* calculated by Maroulis and Thakkar,[7] Bishop and Lam,[8] and by Cernusak et al.[9] led to our reconsideration of the van der Waals moments as a possible explanation for the work function shift in the case of argon on magnesium, where the work function is about 0.5 eV below the first atomic excited-state ionization energy.

In addition, we have included estimates of the effects of several-atom interactions. These effects turn out to be small despite the large number of contributing terms; they also tend to reduce the dipole moment very slightly. The induced moment obtained is consistent with that needed to explain the work-function shift of magnesium in the presence of a monolayer of argon or xenon.

In section II, we develop the formal expressions in terms of the Coulomb operators and charge-density susceptibilities. Following this formal section, in section III, we introduce the image method, and expanding the Coulomb interaction in T-tensors, we apply the results to argon and xenon on palladium and on magnesium. In the last section, we discuss our results.

II. Theoretical Development

Equation 4 of paper I[3] is an expression of the van der Waals induced dipole moment in terms of charge-density susceptibilities of two interacting systems A and B.The relation of this formulation to the more standard approach obtained from the Raleigh−Schrodinger perturbation theory is indicated. In paper I, system A always denoted a molecule (atom); system B could be a molecule (atom) or a solid (metal especially). The treatment there was not confined to nonpolar molecular systems but could include molecules with permanent moments.

† Part of the special issue "George S. Hammond & Michael Kasha Festschrift".

* To whom correspondence should be addressed. Department of Chemistry and Biochemistry. E-mail: linder@chem.fsu.edu. Tel: (850) 644-5299. Fax: (850) 644-8281.

‡ Department of Physics.

10.1021/jp0217334 CCC: $25.00
Published on Web 01/24/2003

In this paper, we rederive the two-body susceptibility formulation using a reaction-field approach[10] developed earlier for the treatment of intermolecular forces. This approach makes it easier to generalize the treatment to three- and four-body interactions, which is one of the main features of our investigation. In this paper, as in the first one, A will always denote the molecule on which the dipole moment is induced. B can be a molecule or a solid; C and D are other molecules adsorbed on the surface, which interact with A and B and each other. Our treatment here is confined to nonpolar molecules, and the induced dipole could be more appropriately described as a dispersion-induced dipole.

In section II.1, we derive the charge-density susceptibility formulation of the induced dipole moment first for the two-body interaction (part A) and then for the extension to include three- and four-body interactions (part B). In section II.2, we describe the theory in terms of the linear and quadratic polarizabilities and T-tensors, which is more practical although less accurate than the susceptibility treatment. In section II.3, we use the image method to describe the induced moment of molecules adsorbed on a surface in terms of the dielectric constant of the solid, polarizabilities, and hyperpolarizabilities of the molecules.

II.1. Charge-Density Susceptibility Formulation. A. Two-Body Interaction. Consider a fluctuation in B at $\mathbf{r}_2''$ and time t'' with charge density $\rho(\mathbf{r}_2'', t'')$ to propagate to A via the potential $V(\mathbf{r}_2'', \mathbf{r}_1'')$, polarizing A and causing a response at $\mathbf{r}_1$ (inducing a moment) and returning via $V(\mathbf{r}_1', \mathbf{r}_2')$ to B at the charge density $\rho(\mathbf{r}_2', t')$. The induced moment can be calculated by considering a hypothetical process whereby the charge at $\mathbf{r}_2'$ increases reversibly from zero to its full value by means of a parameter λ that runs from 0 to 1. Since $\rho(\mathbf{r}_2')$ is linearly dependent on the charge, we have $d\rho(\lambda) = \rho(\lambda = 1)\, d\lambda$.The induced dipole moment at A caused by the fluctuations at B may be described by

$$\mu_{A\leftarrow B} = \int d\mathbf{r}_1 \int d\mathbf{r}_1' \int d\mathbf{r}_1 \int d\mathbf{r}_2' \int d\mathbf{r}_2'' \int_{-\infty}^{t} dt' \int_{-\infty}^{t'} dt'' \int_0^1 d\lambda^B \rho(\mathbf{r}_2', t'; \lambda = 1)\, V(\mathbf{r}_2', \mathbf{r}_1')$$

$$*\mathbf{r}_1\, {}^A\chi^{(2)}(\mathbf{r}_1; \mathbf{r}_1', t - t'; \mathbf{r}_1'', t' - t'')\, V(\mathbf{r}_1'', \mathbf{r}_2'')^B \rho(\mathbf{r}_2'', t''; \lambda) \quad (2\text{-}1a)$$

$$= \int d\mathbf{r}_1 \int d\mathbf{r}_1' \int d\mathbf{r}_1 \int d\mathbf{r}_2' \int d\mathbf{r}_2'' \int_{-\infty \mathrm{bu} > t} dt' \int_{-\infty}^{t'} dt''\, \mathbf{r}_1\, {}^A\chi^{(2)}(\mathbf{r}_1; \mathbf{r}_1', t - t'; \mathbf{r}_1'', t' - t'')$$

$$*V(\mathbf{r}_1'', \mathbf{r}_2'')*V(\mathbf{r}_1', \mathbf{r}_2')* \int_0^1 d\lambda\, {}^1/_2[{}^B\rho(\mathbf{r}_2'', t''; \lambda), {}^B\rho(\mathbf{r}_2', t'; \lambda = 1)]_+ \quad (2\text{-}1b)$$

(We have used the symmetric form of the product of the ${}^B\rho$'s in eq 2-1b because these operators do not commute). The times are arranged so that $t > t' > t''$. Fourier decomposing the integrand, using adiabatic switch-on perturbation $e^{i\omega' t''} e^{\epsilon t'}$ and $e^{i\omega' t''} e^{\eta t''}$, yields

$${}^A\mu_{A\leftarrow B} = {}^1/_2 \int_{-\infty}^{\infty} d\omega \int_{-\infty}^{\infty} d\omega' \int d\mathbf{r}_1 \int d\mathbf{r}_1' \int d\mathbf{r}_1'' \int d\mathbf{r}_2' \int d\mathbf{r}_2'' \langle \mathbf{r}_1 * V(\mathbf{r}_1'', \mathbf{r}_2'')*V(\mathbf{r}_2', \mathbf{r}_1')* {}^A\chi^2(\mathbf{r}_1; \mathbf{r}_1', \omega; \mathbf{r}_1'', \omega')*{}^1/_2[\rho(\mathbf{r}_2'', \omega'), \rho(\mathbf{r}_2', \omega)]_+ e^{i(\omega' + \omega)t} e^{(\xi + \eta)t} \rangle \quad (2\text{-}2)$$

where

$${}^A\chi^{(2)}(\mathbf{r}_1; \mathbf{r}_1', \omega; \mathbf{r}_1'', \omega') = \lim_{\substack{\eta \to 0 \\ \delta \to 0}} \int d\tau \int d\tau' \, {}^A\chi^{(2)}(\mathbf{r}_1; \mathbf{r}_1', \tau; \mathbf{r}_1'', \tau')\, e^{-i(\omega + \omega')\tau} e^{-(\xi + \eta)\tau} e^{-i\omega'\tau'} e^{-\eta\tau'}$$

and $\tau = t - t'$, $\tau' = t' - t''$.

If ${}^A\mu_{A\leftarrow B}$ is to be time-independent, the frequencies ω and ω' have to be equal and opposite, or more precisely, they have to be related by a δ function. Following Landau and Lifshitz,[11] we define

$${}^1/_2\langle [{}^B\rho(\mathbf{r}_2'', \omega'), \rho(\mathbf{r}_2', \omega)]_+ \rangle = [\rho(\mathbf{r}_2'')\, \rho(\mathbf{r}_2')]_\omega\, \delta(\omega + \omega') \quad (2\text{-}3)$$

Integrating out the ω', which replaces (ω') by $(-\omega)$, switching the integration limits of ω from $(-\infty, \infty)$ to $(0, \infty)$, which requires multiplication by 2, and applying the Callen−Welton equation[12]

$$\hbar/2\pi\{\mathrm{Im}^B\chi^{(1)}(\mathbf{r}_2', \mathbf{r}_2, \omega)\} \coth \hbar\omega/2kT = [\rho(\mathbf{r}_2'')\, \rho(\mathbf{r}_2')]_\omega \quad (2\text{-}4)$$

we obtain

$${}^A\mu_{A\leftarrow B} = \int_0^\infty d\omega \int d\mathbf{r}_1 \int d\mathbf{r}_1' \int d\mathbf{r}_1'' \int d\mathbf{r}_2' \int d\mathbf{r}_2'' \langle \mathbf{r}_1 V(\mathbf{r}_1'', \mathbf{r}_2'')\, V(\mathbf{r}_1', \mathbf{r}_2')*\{\mathrm{Re}\, {}^A\chi^{(2)}(\mathbf{r}_1; \mathbf{r}_1', \omega; \mathbf{r}_1'', -\omega)\}*\hbar/2\pi\{\mathrm{Im}^B\chi^{(1)}(\mathbf{r}_2'; \mathbf{r}_2'', \omega)\}* \coth \hbar\omega/2kT \rangle \quad (2\text{-}5)$$

The designation Re and Im refer to the real and imaginary parts of the charge-density susceptibilities. In the original integration over $d\omega$ from $-\infty$ to ∞, only the even or real part of $\chi^{(2)}$ contributes.

The linear and quadratic complex charge-density susceptibilities are given below:

$$\chi^{(1)}(\mathbf{r}; \mathbf{r}', \omega) = \lim_{\xi \to 0} \hbar^{-1} \sum_n [\rho_{0n}(\mathbf{r}')\, \rho_{n0}(\mathbf{r})/(\omega + \omega_{0n} - i\xi) - \rho_{0n}(\mathbf{r})\, \rho_{n0}(\mathbf{r}')/(\omega - \omega_{0n} - i\xi)] \quad (2\text{-}6)$$

$$\chi^{(2)}(\mathbf{r}; \mathbf{r}', \omega; \mathbf{r}'', \omega' = -\omega) = [1 + P(\mathbf{r}', \omega; \mathbf{r}'', \omega')]*\lim_{\xi \to 0} \hbar^{-2} \sum_k \sum_n \{2\rho_{0k}(\mathbf{r})\, \rho_{kn}(\mathbf{r}')\, \rho_{n0}(\mathbf{r}'')/[\omega_{0k}(\omega_{0n} + \omega - i\xi)] + \rho_{0k}(\mathbf{r}')\rho_{kn}(\mathbf{r})\rho_{n0}(\mathbf{r}'')/[\omega_{0k} + \omega - i\xi)(\omega_{0n} + \omega - i\xi)\} \quad (2\text{-}7)$$

where P is an operator that permutes simultaneously the position vectors and the frequencies.

An expression similar to ${}^A\mu_{A\leftarrow B}$, namely, ${}^A\mu_{B\leftarrow A}$ with the Re and Im designation interchanged, represents polarization originating from fluctuations in A. Together they constitute the induced moment in A:

$${}^A\mu = {}^A\mu_{BA} + {}^A\mu_{AB} = \hbar/2\pi\ \mathrm{Re}\ i \int d\mathbf{r}_1 \int d\mathbf{r}_1' \int d\mathbf{r}_1'' \int d\mathbf{r}_2' \int d\mathbf{r}_2'' *\langle \mathbf{r}_1 V(\mathbf{r}_1'', \mathbf{r}_2'')\, V(\mathbf{r}_1', \mathbf{r}_2') \int_0^\infty d\omega\, {}^A\chi^{(2)}(\mathbf{r}_1; \mathbf{r}_1', \omega; \mathbf{r}_1'', -\omega)* {}^B\chi^{(1)}(\mathbf{r}_2''; \mathbf{r}_2', \omega)\rangle \quad (2\text{-}8)$$

The result in eq 2-5 in terms of the hyperbolic cotangent is applicable to both quantal and classical regimes. In the strict quantal limit ($T = 0$) in which we are interested here, $\coth \hbar\omega/2kT \to 1$.

Although the theory is formally complete, it is convenient to express the results in terms of frequencies along the negative axis of the complex frequency plane; there the susceptibilities are real. Thus, if we replace ω by $f = \omega - iy$ and ω' by $f' = \omega' - iy = -\omega - iy$ and integrate along the imaginary axis, we have

$$^{A}\mu = \hbar/2\pi \int d\mathbf{r}_1 \int d\mathbf{r}_1' \int d\mathbf{r}_1'' \int d\mathbf{r}_2' \int d\mathbf{r}_2'' \, {}^{*}\mathbf{r}_1 \, {}^{*}V(\mathbf{r}_1'', \mathbf{r}_2'')^{*} \, V(\mathbf{r}_1', \mathbf{r}_2')^{*} \int_0^\infty dy \, {}^{A}\chi^{(2)}(\mathbf{r}_1; \mathbf{r}_1', -iy; \mathbf{r}_1'', -iy)^{*} {}^{B}\chi^{(1)}(\mathbf{r}_2''; \mathbf{r}_2', -iy) \quad (2\text{-}9)$$

where

$$\chi^{(1)}(\mathbf{r}''; \mathbf{r}', -iy) = 2/\hbar \sum_n{}' \, \omega_{0n} \rho_{0n}(\mathbf{r}'') \, \rho_{n0}(\mathbf{r})/(\omega_{0n}{}^2 + y^2) \quad (2\text{-}10a)$$

$$\chi^{(2)}(\mathbf{r}''; \mathbf{r}', -iy; \mathbf{r}, -iy) = 1/\hbar^2[1 + P(\mathbf{r}', -iy; \mathbf{r}, -iy)]^{*} \sum_n \sum_k \{2\rho_{0k}(\mathbf{r}'') \, \rho_{kn}(\mathbf{r}') \, \rho_{n0}(\mathbf{r}) \, \omega_{0n}/[\omega_{0k}(\omega_{0n}{}^2 + y^2)] + \rho_{0k}(\mathbf{r}') \, \rho_{kn}(\mathbf{r}'') \, \rho_{n0}(\mathbf{r}) \, (\omega_{0k}\omega_{0n} - y^2)/[(\omega_{0k}{}^2 + y^2)(\omega_{0n}{}^2 + y^2)]\} \quad (2\text{-}10b)$$

B. Generalization to 3- and 4-Body Interactions. The reaction potential procedure for generating the induced dipole moment on A can readily be generalized to include other molecules. In the presence of a third body, C, we may visualize a fluctuation that starts at ${}^{C}\rho(\mathbf{r}_3''', t''')$ of molecule C, propagates via $V(\mathbf{r}_3''', \mathbf{r}_2'')$ to B, polarizes it causing a fluctuation that propagates via $V(\mathbf{r}_2'', \mathbf{r}_1'')$ to A where it polarizes A, producing an induced moment at $\rho(\mathbf{r}_1)$, and a charge fluctuation that propagates via $V(\mathbf{r}_1', \mathbf{r}_3'')$ to C. For any given configuration, the result is the same for the route C → B → A as for C → A → B, so only one route need be considered, and the result has to be multiplied by 2.

In the presence of C and D, starting with D, there are six permutations among A, B, and C, and thus the final result has to be multiplied by 6.

The induced dipole moment due to the two-body and nonadditive three-body and four-body interactions can now be written

$$^{A}\mu = \hbar/2\pi \int d\mathbf{r}_1 \int d\mathbf{r}_1' \int d\mathbf{r}_1'' \int d\mathbf{r}_2' \int d\mathbf{r}_2'' \, \mathbf{r}_1 \, V(\mathbf{r}_1'', \mathbf{r}_2'') \, V(\mathbf{r}_1', \mathbf{r}_2') \, {}^{*} \int_0^\infty dy \, {}^{A}\chi^{(2)}(\mathbf{r}_1; \mathbf{r}_1', -iy; \mathbf{r}_1'', -iy) \, {}^{B}\chi^{(1)}(\mathbf{r}_2''; \mathbf{r}_2', -iy)$$

$$+ \hbar/\pi \int d\mathbf{r}_1 \int d\mathbf{r}_1' \int d\mathbf{r}_1'' \int d\mathbf{r}_2' \int d\mathbf{r}_2'' \int d\mathbf{r}_3' \int d\mathbf{r}_3'' \, \mathbf{r}_1 \, V(\mathbf{r}_3', \mathbf{r}_2') \, V(\mathbf{r}_1'', \mathbf{r}_2'') \, V(\mathbf{r}_3'', \mathbf{r}_1') \, {}^{*} \int_0^\infty dy \, {}^{A}\chi^{(2)}(\mathbf{r}_1; \mathbf{r}_1', -iy; \mathbf{r}_1'', -iy) \, {}^{B}\chi^{(1)}(\mathbf{r}_2''; \mathbf{r}_2', -iy) \, {}^{*C}\chi^{(1)}(\mathbf{r}_3'; \mathbf{r}_3'', -iy)$$

$$+ 3\hbar/\pi \int d\mathbf{r}_1 \int d\mathbf{r}_1' \int d\mathbf{r}_1'' \int d\mathbf{r}_2' \int d\mathbf{r}_2'' \int d\mathbf{r}_3' \int d\mathbf{r}_3'' \int d\mathbf{r}_4' \int d\mathbf{r}_4'' \, \mathbf{r}_1 \, {}^{*}V(\mathbf{r}_3', \mathbf{r}_2') \, V(\mathbf{r}_1'', \mathbf{r}_2'') \, V(\mathbf{r}_3'', \mathbf{r}_4') \, V(\mathbf{r}_4'', \mathbf{r}_1') \, {}^{*} \int_0^\infty dy \, {}^{A}\chi^{(2)}(\mathbf{r}_1; \mathbf{r}_1', -iy; \mathbf{r}_1'', -iy) \, {}^{B}\chi^{(1)}(\mathbf{r}_2''; \mathbf{r}_2', -iy) \, {}^{C}\chi^{(1)}(\mathbf{r}_3'; \mathbf{r}_3'', -iy) \, {}^{D}\chi^{(1)}(\mathbf{r}_4'; \mathbf{r}_4'', -iy) \quad (2\text{-}11)$$

II.2. (Hyper)polarizabilty Formulation. If we expand the Coulomb potential $V(\mathbf{r}_1, \mathbf{r}_2)$ in a multipole series,[3,13] we obtain an expression in terms of moment operators and T tensors. From the coupling of the moments with the charge-density susceptibilities, one obtains the (hyper)polarizabilities. The most important polarizabilities for a system of nonpolar molecules are the ordinary dipole−dipole polarizability, α, and the dipole−dipole quadrupole hyperpolarizability *B*. Along the imaginary frequency axis, these polarizabilities take the form

$$\alpha_{\beta\gamma} = -\int d\mathbf{r} \int d\mathbf{r}' \, r_\beta \chi^{(1)}(\mathbf{r}; \mathbf{r}', -iy) \, r_\gamma' \quad (2\text{-}12)$$

$$B_{\lambda\beta\gamma\delta}(-iy, -iy) = \int d\mathbf{r} \int d\mathbf{r}' \int d\mathbf{r}'' \, r_\lambda \chi^{(2)}(\mathbf{r}; \mathbf{r}', -iy; \mathbf{r}'', -iy) \, \theta_{\beta\gamma}(\mathbf{r}') \, r_\delta'' \quad (2\text{-}13)$$

where $\theta_{\beta\gamma} = {}^1/_2(3r_\beta r_\gamma - r^2\delta_{\beta\gamma})$ is the quadrupole moment operator. Denoting the second- and third-rank T-tensor components, respectively, as $T_{\beta\epsilon}^{(2)}$(A, B) and $T_{\eta\gamma\delta}^{(3)}$(C, A) where the capital letters refer to the molecules A, B, et cetera, we obtain for the hyperpolarizability formulation of the two-, three- and four-body induced moment, analogous to eq 2-11,

$$^{A}\mu_\lambda = \hbar/2\pi T_{\beta\epsilon}^{(2)}(A, B) \int_0^\infty dy \, {}^{A}B_{\lambda\beta\gamma\delta}(-iy, -iy) \, {}^{B}\alpha_{\beta\epsilon}(-iy) + \hbar/\pi P(B, C)[T_{\beta\epsilon}^{(2)}(A, B) \, T_{\epsilon\eta}^{(2)}(B, C) \, T_{\eta\gamma\delta}^{(3)}(C, A) \times \int_0^\infty dy \, {}^{A}B_{\lambda\beta\gamma\delta}(-iy, -iy) \, {}^{B}\alpha_{\beta\epsilon}(-iy) \, {}^{C}\alpha_{\epsilon\eta}(-iy)] + 3\hbar/\pi P(B, C, D)[T_{\beta\epsilon}^{(2)}(A, B) \, T_{\epsilon\eta}^{(2)}(B, C) \, T_{\eta\xi}^{(2)}C, D) \, T_{\xi\beta\delta}^{(3)}(D, A) \times \int_0^\infty dy \, {}^{A}B_{\lambda\beta\gamma\delta}(-iy, -iy) \, {}^{B}\alpha_{\beta\epsilon}(-iy) \, {}^{C}\alpha_{\epsilon\eta}(-iy) \, {}^{D}\alpha_{\eta\xi}(-iy)] \quad (2\text{-}14)$$

Repeated tensor indices imply summations over *x*, *y*, and *z*.

P refers to the permutation of molecules in its arguments. Term 1 is the induced moment on A by the van der Waals interaction with B. Eventually, B will be treated as a solid, and thus the first term is the moment induced in A by the solid. The second term represents a nonadditive contribution due to the presence of one additional molecule. The last term represents the nonadditive contribution due to two additional molecules. The contributions to the moment will be later referred to respectively as M_1, M_2, and M_3.

II.3. Image Method. We employ for atom 1 a coordinate system $\mathbf{r}_1$, $\mathbf{r}_1'$, $\mathbf{r}_1''$ centered on the atomic nucleus. Since we are neglecting exchange and charge transfer, we assume that the atomic nuclei are separated from the image plane of the metal by a distance Z_0, which we choose to be the collision radius r_v + 0.7 Å, and from the nearest atomic nucleus by $2r_v$. The added 0.7 Å is a somewhat arbitrarily chosen "screening length" to allow for the image plane of the metal being below the adsorption surface.[14]

If the atom 1 has a charge density $\rho(\mathbf{r}_1')$ at a point $\mathbf{r}_1 = x_1'\mathbf{i} + y_1'\mathbf{j} + z_1'\mathbf{k}$,, then the effect of a dielectric solid is to produce an image charge $-\rho(\mathbf{r}_1')((\epsilon - 1)/(\epsilon + 1))$ located at a point $\tilde{\mathbf{r}}_1'$; as far below the surface as the point $\mathbf{r}_1'$ is above, on a line perpendicular to the surface through $\mathbf{r}_1'$; ϵ is the dielectric constant. In this paper, we choose the *z* axis (direction of **k**)

along this line in the direction from the surface to atom l. Thus, the image charge is located at

$$\tilde{\mathbf{r}}_1' = \mathbf{r}_1' - 2\mathbf{k}(Z_0 + z_1') \text{ or}$$
$$= x_1'\mathbf{i} + y_1'\mathbf{j} - (2Z_0 + z_1')\mathbf{k} \qquad (2-15)$$

Thus, a combination such as (we temporarily ignore the frequency dependences)

$$\rho(\mathbf{r}_1')\, V(\mathbf{r}_1', \mathbf{r}_2')\, {}^{B}\chi^{(1)}(\mathbf{r}_2'; \mathbf{r}_2'')\, V(\mathbf{r}_2'', \mathbf{r}_3')\, {}^{C}\chi^{(1)}(\mathbf{r}_3'; \mathbf{r}_3'')$$

would become

$$-\left(\frac{\epsilon - 1}{\epsilon + 1}\right)\rho(\mathbf{r}_1')\, V(\tilde{\mathbf{r}}_1', \mathbf{r}_3')\, {}^{C}\chi^{(1)}(\mathbf{r}_3', \mathbf{r}_3'')$$

The charge density $\rho(\mathbf{r}_1')$ is, of course, actually a part of $\chi^{(1)}$ or $\chi^{(2)}$. The frequency dependence of $((\epsilon - 1)/(\epsilon + 1))$ is assumed to be the same as that of ${}^{B}\chi^{(1)}$ except that the excitation frequency is replaced by the plasma frequency divided by $\sqrt{2}$ in the closure approximation in the metallic limit[2c] where $((\epsilon(0) - 1)/(\epsilon(0) + 1)) \rightarrow 1$.

Thus, by choosing B to represent the solid, we can relate the charge density susceptibility of B to the dielectric constant of the solid by substituting the image form

$$\int d\mathbf{r}_2' \int d\mathbf{r}_2\, {}^{B}\chi^{(1)}(\mathbf{r}_2; \mathbf{r}_2', -iy)\, V(\mathbf{r}_1\mathbf{r}_2)\, V(\mathbf{r}_2'\mathbf{r}) =$$
$$[\epsilon(-iy) - 1]/[\epsilon(-iy) + 1]\, V(\tilde{\mathbf{r}}'_1, \mathbf{r}) \quad (2\text{-}16)$$

If we expand V in eq 2-16 in a multipole series, we obtain for a nonpolar molecule adsorbed on a surface

$$M_1 = 3\hbar/(8\pi Z_0^4) \int_0^\infty dy\, [\epsilon(-iy) - 1]/[\epsilon(-iy) + 1] \times$$
$$[3\,{}^{A}B_{\lambda zzz}(-iy, -iy) + 2\,{}^{A}B_{\lambda xzx}(-iy, -iy) +$$
$$2\,{}^{A}B_{\lambda yzy}(-iy, -iy)] \quad (2\text{-}17)$$

For a spherical atom, $B_{zxzx} = B_{zyzy} = {}^{3}/_{4}B_{zzzz}$.

The expressions for the nonadditive terms M_2 and M_3 are much more complicated and are discussed in some detail in the section on applications.

III. Application to an Adsorbed Monolayer on the Plane Surface of a Metal

The system to which we apply the results of the preceding section is a square lattice of argon (or xenon) atoms physadsorbed as a monolayer on the plane surface of a semi-infinite solid. We identify system B of the previous section as the solid and the noble gas atoms as systems A, C, D, et cetera. To avoid the complications of treating B in detail, we will utilize the image approximation, as we have previously.[2c,3] For this reason, we treat the "order of interaction" as equal to the number of atoms involved regardless of the number of images included.

Finally, we have expanded the interactions remaining after applying the image approximation in the usual T-tensor expansion and have carried out the integrations over the atomic coordinates by recognizing the polarizabilities and hyperpolarizabilities as the appropriate integrals over the charge density susceptibilities.[3]

The imaginary frequency dependences of α and B are the same as those of $\chi^{(1)}$ and $\chi^{(2)}$, respectively. As we did in our 1986 paper,[3] we will approximate these in closure,

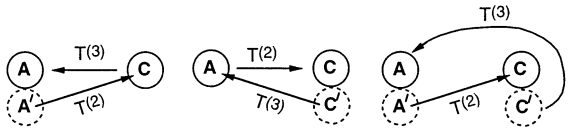

Figure 1. Schematic of the interactions in the two-atom terms. Images are shown by dotted circles and primed letters, and atoms are shown by solid-line circles and no primes.

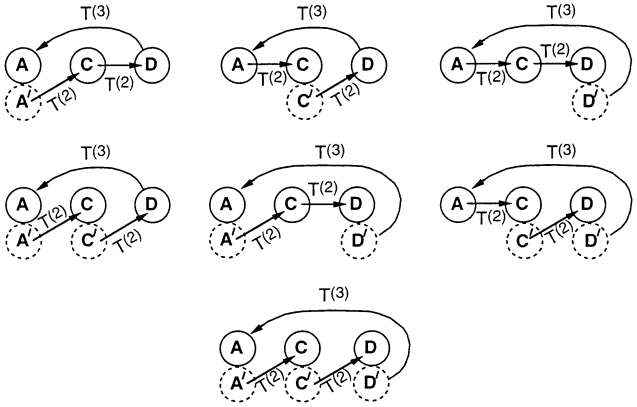

Figure 2. Schematic of the interactions in the three-atom terms. Symbols are the same as those in Figure 1.

which enables us to write α and B as their zero-frequency values multiplied by a frequency factor. This greatly simplifies the integration of our expressions over imaginary frequencies and enables the effect of this integration to be condensed into a numerical factor multiplied by an expression that involves only zero-frequency values of α, B, and $((\epsilon - 1)/(\epsilon + 1))$.

The terms involving ${}^{C}\alpha$, ${}^{D}\alpha$, ${}^{A}B$ are the lowest-order terms surviving the T-tensor expansion; we have not considered higher-order hyperpolarizabilities because we expect such terms to be relatively small and because the hyperpolarizabilities are not known. Indeed, only in recent years have reliable values of B become available for noble gases.

The inclusion of an additional atom in a term contributing to the dipole moment of atom A reduces that contribution by about 1 order of magnitude, as we shall see. However, we find that including an additional interaction of the metal with a previously unimaged atom in the original term reduces the term by roughly a factor of 3 on the average (and occasionally *increases* it) and changes the sign.

As shown in Figures 1 and 2, there are three types of terms for two-atom interactions differing in the imaging process included, and there are seven types of three-atom terms. Also, in a lattice of N^2 atoms, there are $(N^2 - 1)$ configurations for each two-atom term type and $(N^2 - 1)(N^2 - 2)$ configurations for each three-atom term type. (Atom A, whose dipole moment is being calculated as representative of an arbitrarily chosen atom in an infinite lattice, is fixed for convenience at the center of the lattice.) N is always chosen to be odd, and the lattice sums are taken over the atoms in a circle, centered on A, of radius $(N - 1)r_v$. The value of N is increased until the sums are independent of N to three figures. Despite the rapid increase in the number of terms as N increases, the sum is essentially constant for $N \geq 15$. As stated in section II, we designate the one-atom term as M_1, the two-atom nonadditive terms as M_2, and the three-atom nonadditive terms as M_3. We have not calculated terms involving larger numbers of atoms, but we

believe that they will be relatively small. The single-atom contribution is

$$M_1 = \left(\frac{1}{2\pi}\right)\left(\frac{1}{3}I_{11}\right)\{B_{zzzz}T^{(3)}_{z,zz}(A', A) + B_{zzxx}T^{(3)}_{z,xx}(A', A) + B_{zzyy}T^{(3)}_{z,yy}(A', A) - B_{zxzx}T^{(3)}_{x,zx}(A', A) - B_{zyzy}T^{(3)}_{y,zy}(A', A) - B_{zxxz}T^{(3)}_{x,xz}(A', A) - B_{zyyz}T^{(3)}_{y,yz}(A', A)\} \quad (3\text{-}4)$$

where the symbols (A′, A) indicate that the displacement vector from the center of the image of atom A to the center of atom A is used to calculate $T^{(3)}$. I_{11} is $\hbar$ times the integral over the imaginary frequencies and has the dimensions of energy. The frequency integrals are defined below. The B's in the above expression are the zero-frequency B's.

For single-image terms corresponding to the first diagram in Figure 1, the M_2 terms are

$$\begin{aligned} M_2 = \alpha\{&B_{zzzz}[T^{(2)}_{zz}(A', C)\,T^{(3)}_{zzz}(C, A) + T^{(2)}_{zx}(A', C)\,T^{(3)}_{x,zz}(C, A) + T^{(2)}_{zy}(A',C)\,T^{(3)}_{y,zz}(C, A)] + \\ &B_{zzxx}[T^{(2)}_{zz}(A', C)\,T^{(3)}_{z,xx}(C, A) + T_{zx}{}^{(2)}(A', C)\,T^{(3)}_{x,xx}(C, A) + T^{(2)}_{zy}(A', C)\,T^{(3)}_{y,xx}(C, A)] + \\ &B_{zzyy}[T^{(2)}_{zz}(A', C)\,T^{(3)}_{z,yy}(C, A) + T^{(2)}_{zx}(A', C)\,T^{(3)}_{x,yy}(C, A) + T^{(2)}_{zy}(A', C)\,T^{(3)}_{y,yy}(C, A)] - \\ &B_{zxzx}[T^{(2)}_{xz}(A', C)\,T^{(3)}_{z,zx}(C, A) + T^{(2)}_{xx}(A', C)\,T^{(3)}_{x,zx}(C, A) + T^{(2)}_{xy}(A', C)\,T^{(3)}_{y,zx}(C,A)] - \\ &B_{zyzy}[T^{(2)}_{yz}(A', C)\,T^{(3)}_{z,zy}(C, A) + T^{(2)}_{yx}(A', C)\,T^{(3)}_{x,zy}(C, A) + T^{(2)}_{yy}(A', C)\,T^{(3)}_{y,zy}(C, A)] - \\ &B_{zxxz}[T^{(2)}_{xz}(A', C)\,T^{(3)}_{z,yz}(C, A) + T^{(2)}_{xx}(A', C)\,T^{(3)}_{x,xz}(C, A) + T^{(2)}_{xy}(A', C)\,T^{(3)}_{y,xz}(C, A)] - \\ &B_{zyyz}[T^{(2)}_{yz}(A', C)\,T^{(3)}_{z,xz}(C, A) + T^{(2)}_{yx}(A', C)\,T^{(3)}_{x,yz}(C, A) + T^{(2)}_{yy}(A', C)\,T^{(3)}_{y,yz}(C, A)]\}\left(\frac{I_{21}}{6\pi}\right) \end{aligned} \quad (3\text{-}5)$$

where I_{21} is an integral over the imaginary frequencies and the α and B are at zero frequency.

We have included in eq 3-1 the seven nonzero components of $B_{z\alpha\beta\gamma}$ for a spherical atom. In the evaluation, we have used the relations between these seven and B_{zzzz} given in our previous paper: $B_{zzxx} = B_{zzyy} = (-1/2)B_{zzzz}$ and all others equal $3/4 B_{zzzz}$. Also, for a spherical atom, we have dropped the component subscripts on α since there are only three equal diagonal components.

The prime on A indicates that the displacement vector from the image of A to atom C is used to calculate the components of $T^{(2)}$, whereas the displacement from atom C to atom A is used to calculate $T^{(3)}$. As in eq 3-4 above, the negative sign on the terms utilizing $B_{zx\beta\gamma}$ and $B_{zy\beta\gamma}$ reflects the reversal of the x and y components of dipoles by imaging whereas the $B_{zz\beta\gamma}$ terms are not negative because the z components of dipoles are not reversed by imaging.

By similar reasoning, the two-atom terms corresponding to the second diagram in Figure 1 are

$$\begin{aligned} M_2 = \alpha\{&B_{zzzz}[T^{(2)}_{zz}(A, C)\,T^{(3)}_{z,zz}(C', A) - T^{(2)}_{zx}(A, C)\,T^{(3)}_{x,zz}(C', A) - T^{(2)}_{zy}(A, C)\,T^{(3)}_{y,zz}(C', A)] + \\ &B_{zzxx}[T^{(2)}_{zz}(A, C)\,T^{(3)}_{z,xx}(C', A) - T^{(2)}_{zx}(A', C)\,T^{(3)}_{x,xx}(C', A) - T^{(2)}_{zy}(A, C)\,T^{(3)}_{y,xx}(C', A)] + \\ &B_{zzyy}[T^{(2)}_{zz}(A, C)\,T^{(3)}_{z,yy}(C', A) - T^{(2)}_{zx}(A, C)\,T^{(3)}_{x,yy}(C', A) - T^{(2)}_{zy}(A, C)\,T^{(3)}_{y,yy}(C', A)] + \\ &B_{zxzx}[T^{(2)}_{xz}(A, C)\,T^{(3)}_{z,zx}(C', A) - T^{(2)}_{xx}(A, C)\,T^{(3)}_{x,zx}(C', A) - T^{(2)}_{xy}(A, C)\,T^{(3)}_{y,zx}(C', A)] + \\ &B_{zyzy}[T^{(2)}_{yz}(A, C)\,T^{(3)}_{z,zy}(C', A) - T^{(2)}_{yx}(A, C)\,T^{(3)}_{x,zy}(C', A) - T^{(2)}_{yy}(A, C)\,T^{(3)}_{y,zy}(C', A)] + \\ &B_{zxxz}[T^{(2)}_{xz}(A, C)\,T^{(3)}_{z,xz}(C', A) - T^{(2)}_{xx}(A, C)\,T^{(3)}_{x,xz}(C', A) - T^{(2)}_{xy}(A, C)\,T^{(3)}_{y,xz}(C', A)] + \\ &B_{zyyz}[T^{(2)}_{yz}(A, C)\,T^{(3)}_{z,xz}(C', A) - T^{(2)}_{yx}(A, C)\,T^{(3)}_{x,yz}(C', A) - T^{(2)}_{yy}(A, C)\,T^{(3)}_{y,yz}(C', A)]\}\left(\frac{I_{21}}{6\pi}\right) \end{aligned} \quad (3\text{-}6)$$

The two image terms are like those in eq 3-6 except the coefficients of B_{zxzx}, B_{zyzy}, B_{zxxz}, and B_{zyyz} are negative, the $T^{(2)}$-(A, C) terms are replaced by $T^{(2)}$(A′, C) terms as in eq 3-4, and I_{21} is replaced by I_{22}.

We do not display explicitly the seven term types for the three-atom terms, but the logic is the same.

The last thing to be discussed in this section is the integration over the imaginary frequencies. We approximate the frequency dependence of the various factors by closure. The frequency dependence of the dipole−dipole polarizability α becomes $(\bar{\omega}^2/(\bar{\omega}^2 + y^2))$, where $\bar{\omega}$ is the effective excitation frequency; the frequency dependence of the factor $((\epsilon - 1)/(\epsilon + 1))$ becomes $([(1/2)\omega_p{}^2]/[(1/2)(\omega_p{}^2 + y^2)])$, where ω_p is the plasma frequency of the metal, and the frequency dependence of B becomes $1/3\, f(y)$, where

$$f(y) = \frac{2\bar{\omega}^2}{\bar{\omega}^2 + y^2} + \frac{\bar{\omega}^2(\bar{\omega}^2 - y^2)}{(\bar{\omega}^2 + y^2)^2} \quad (3\text{-}7)$$

Thus, the frequency integral for a term involving n atoms and l images is, apart from the factor of $(1/3)$ mentioned above,

$$I_{nl} = \hbar\int_0^\infty dy\, f(y)\left(\frac{\bar{\omega}^2}{\bar{\omega}^2 + y^2}\right)^{n-1}\left(\frac{\frac{1}{2}\omega_p^2}{\frac{1}{2}\omega_p^2 + y^2}\right)^{l} \quad (3\text{-}8)$$

Although it is possible to carry out these integrals in closed form, we have evaluated them numerically with the aid of Maple 7 software.

IV. Results

The values of the dipole−dipole polarizability α and the dipole−dipole−quadrupole hyperpolarizability B for argon were taken from Cernusok, Diercksen, and Sadlej,[9]

$$\alpha = 11.07 \text{ au}$$

$$B_{zzzz} = -167.5 \text{ au}$$

TABLE 1: Frequency Integrals I_{mn} (eV)[a]

		magnesium			palladium		
	n/m	1	2	3	1	2	3
Ar	1	21.72			32.57		
	2	18.82	14.22		25.64	22.48	
	3	16.95	13.36	11.29	21.85	19.32	18.28
Xe	1	19.35			27.39		
	2	16.31	12.96		20.91	18.97	
	3	14.44	11.96	10.39	17.56	16.37	15.45

[a] n is the number of atoms, and m is the number of images.

TABLE 2: Contributions to the Total Dispersion-Induced Moment as a Function of Monolayer Diameter for Argon and Xenon on Magnesium[a,b]

	$N=$	3	5	9	15	25
Ar	$M_2 \times 10^4$	−1.54	−1.89	−1.95	−1.95	−1.95
	$M_3 \times 10^5$	−2.55	−1.94	−1.30	−1.28	−1.28
	$M_1 = 1.11 \times 10^{-2}$ atomic units					
	$M = 1.08 \times 10^{-2}$ atomic units					
Xe	$M_2 \times 10^4$	−6.94	−8.48	−8.71	−8.72	−8.72
	$M_3 \times 10^5$	−18.2	−14.3	−9.92	−9.80	−9.80
	$M_1 = 3.22 \times 10^{-2}$ atomic units					
	$M = 3.12 \times 10^{-2}$ atomic units					

[a] $M = M_1 + M_2 + M_3$. [b] To these figures, M is independent of N for $N \geq 3$. A subscript on M indicates the number of atoms contributing to that term. The monolayer diameter is $(N-1)$ atomic diameters $= 2r_v(N-1)$.

TABLE 3: Contributions to the Total Dispersion-Induced Moment as a Function of Monolayer Diameter for Argon and Xenon on Palladium[a,b]

	$N=$	3	5	9	15	25
Ar	$M_2 \times 10^4$	−2.05	−2.52	−2.60	−2.60	−2.60
	$M_3 \times 10^5$	−3.25	−2.52	−1.70	−1.67	−1.67
	$M_1 = 1.66 \times 10^{-2}$ atomic units					
	$M = 1.63 \times 10^{-2}$ atomic units					
Xe	$M_2 \times 10^4$	−8.72	−10.6	−10.9	−10.9	−10.9
	$M_3 \times 10^5$	−21.9	−17.4	−12.4	−12.2	−12.2
	$M_1 = 4.56 \times 10^{-2}$ atomic units					
	$M = 4.43 \times 10^{-2}$ atomic units					

[a] $M = M_1 + M_2 + M_3$. [b] To three figures, M is independent of N for $N \geq 5$. A subscript on M indicates the number of atoms contributing. The monolayer diameter is $(N-1)$ atomic diameters $= 2r_v(N-1)$.

whereas the values for xenon (in au)

$$\alpha = 27.7$$
$$B_{zzzz} = -812.0$$

were taken from Maroulis and Thakar.[7b] With the exception of the plasma frequency of magnesium, the rest of the data used here was the same as in our 1979 paper.[2d] The plasma frequency of magnesium, 10.9 eV, was taken from Pines.[15]

Table 1 contains the values of the integrals I_{mn} over the negative imaginary frequencies of the terms involving n adsorbed atoms and m interactions between the metal substrate and m of the n atoms in the surface monolayer. The plasma frequency of the metal, ω_p, and the effective excitation level of argon, $\bar{\omega}$, were expressed in electronvolts, so I_{mn} is also in electronvolts.

Tables 2 and 3 contain the contributions to the dispersion-induced moment for an isolated atom of argon, M_1, on magnesium (Table 2) and palladium (Table 3) and the nonadditive two-atom, M_2, and three-atom, M_3, contributions as a function of the size of the monolayer of N atomic diameters.

The contributions have converged to their final values (to three figures) if they are summed over a monolayer including all argon atoms within 15 atomic diameters. Both the two- and three-atom nonadditive contributions reduce the moment, but the two-atom terms increased slightly in magnitude as the size of the monolayer increased whereas the three-atom terms decreased slightly in magnitude. The number of terms in these sums increases rapidly as the size of the monolayer increases, being $7(N^2-1)(N^2-2)$ for the M_3 terms and $3(N^2-1)$ for the M_2 terms.

The total moments can be converted to D by multiplying by the Bohr radius in angstroms times the electronic charge in statcoulombs times 10^{10}. This yields

$$M = 2.74 \times 10^{-2} \text{ D for argon on magnesium}$$
$$M = 7.94 \times 10^{-2} \text{ D for xenon on magnesium}$$
$$M = 4.14 \times 10^{-2} \text{ D for argon on palladium}$$
$$M = 11.25 \times 10^{-2} \text{ D for xenon on palladium}$$

By dividing these M values by the square of the atomic diameter in centimeters, one obtains the dipole moment per unit area, which is equal to $(1/4\pi)$ times the potential step across the layer (and hence the reduction in the work function due to the monolayer) in statvolts, which is easily converted to volts by multiplying by 300:

$$\Delta\phi = \frac{300\pi M}{r_v^2} \tag{4-1}$$

The values obtained are

$$\Delta\phi = 0.0817 \text{ eV, Ar on Mg}$$
$$\Delta\phi = 0.180 \text{ eV, Xe on Mg}$$
$$\Delta\phi = 0.124 \text{ eV, Ar on Pd}$$
$$\Delta\phi = 0.256 \text{ eV, Xe on Pd}$$

The experimental values are 0.10 eV for Ar on Mg and approximately 0.31 eV for Ar on Pd, 0.21 eV for Xe on Mg, and 0.93 eV for Xe on Pd as estimated from the graphs of Chen et al.[5]

V. Discussion

Our calculated work-function reduction for argon and for xenon on magnesium are in good agreement with the values given in the graphs of Chen et al.,[5] considering the approximations we used in our calculations:

The centers of the adsorbed atoms were assumed to be separated from the image plane of the metal by 0.7 Å more than the atomic collision radius. Of course, the use of the image method itself is an approximation. In addition, our model of the argon and xenon lattice is no doubt naïve, which would affect the density of dipole moments in our calculation of the reduction in the work function. What can be said is that the dispersion dipoles can account for the work-function reduction in these cases.

Chen et al.[5] also noted that the work-function reduction of magnesium appeared to be simply proportional to the argon surface coverage; there was no significant reduction of the atomic moment with coverage such as was observed, for example, by Palmberg[16] for xenon on palladium. This is consistent with the small contribution of the nonadditive two- and three-atom terms to our calculated moments: reductions of about 1.1−1.2% for the two-atom terms and 0.07% for the

three-atom terms, indicating a deviation from proportionality of about 1.17−1.27%.

If we consider the calculated and experimental values for the reduction of the palladium work function, then the calculated dispersion reductions are smaller than the experimental values. Or, more generally, the ratio of the work-function reduction for palladium to that for magnesium is about half the experimental ratio.

If we look at the reduction of the moment as a function of the monolayer radius for xenon on palladium, then our calculated reduction per atom as the coverage increases from zero to 1 is less than 2%, just as in the case of magnesium, where the experiments of Palmberg[16] showed a change by a factor of 2. These facts encourage one to believe that dispersion is adequate to explain the work-function reduction on magnesium but that some additional mechanism contributes significantly to the work-function reduction of palladium; this mechanism could be that suggested by Chen et al.,[5,6] for example.

Acknowledgment. It is a pleasure to dedicate this paper in honor of Professor Michael Kasha's 80th birthday. His infinite curiosity about many subjects, not all in chemistry, raises questions that stimulate the mind and give rise to vigorous discussions.

References and Notes

(1) (a) Frommhold, L. *Collision-Induced Absorption in Gases*; Cambridge University Press: Cambridge, U.K., 1993. (b) Li, X.; Champagne, M. H.; Hunt, K. L. C. *J. Chem. Phys.* **1998**, *109*, 8416. (c) Hunt, K. L. C.; Li, X. In *Collision- and Interaction-Induced Spectroscopy*; Tabiaz, G. C., Neuman, M. N., Eds.; NATO ASI Series C; Kluwer: Dordrecht, The Netherlands, 1995; p 452. (d) Linder, B. *Int. J. Quantum Chem.* **1991**, *39*, 437. (e) Linder, B. *J. Phys. Chem.* **1992**, *96*, 1708. (f) Linder, B.; Kromhout, R. A. *Mol. Phys.* **1989**, *67*, 1181.

(2) (a) Crowell, A. D. *J. Chem. Phys.* **1974**, *61*, 33485. (b) Antoniewicz, P. R. *Phys. Rev. Lett.* **1974**, *32*, 1424. (c) Linder, B.; Kromhout, R. A. *Phys. Rev.* **1976**, *12*, 1532. (d) Kromhout, R. A.; Linder, B. *Chem. Phys. Lett.* **1979**, *61*, 283.

(3) Linder, B.; Kromhout, R. A. *J. Chem. Phys.* **1986**, *84*, 2753.

(4) Hunt, K. L. C. *J. Chem. Phys.* **1984**, *80*, 393.

(5) Chen, Y. C.; Cunningham, J. E.; Flynn, C. P. *Phys. Rev. B* **1984**, *30*, 7317.

(6) Flynn, C. P.; Chen, Y. C. *Phys. Rev. Lett.* **1981**, *46*, 447.

(7) (a) Maroulis, G.; Thakkar, A. J. *Chem. Phys. Lett.* **1989**, *156*, 87. (b) Maroulis, G.; Thakkar, A. J. *J. Chem. Phys.* **1988**, *89*, 7320.

(8) Bishop, D. M.; Lam, B. *J Chem. Phys.* **1988**, *88*, 3398.

(9) Cernusak, I.; Diercksen, G. H. F.; Sadlej, A. J. *Chem. Phys. Lett.* **1986**, *128*, 18.

(10) Linder, B.; Rabenold, D. A. *Adv. Quantum Chem.* **1972**, *6*, 203.

(11) Landau, L. D.; Lifschitz, E. M. *Statistical Physics*; Pergamon Press: Oxford, U.K.,1958; Chapter 12.

(12) Callen, H. B.; Welton, T. A. *Phys. Rev.* **1951**, *83*, 34.

(13) Kielich, S. *Physica* **1965**, *31*, 444.

(14) Engel, T.; Gomer, R. *J. Chem. Phys.* **1976**, *52*, 5572.

(15) Pines, D. *Elementary Excitations in Solids*; W. A. Benjamin: New York, 1963.

(16) Palmberg, P. W. *Surf. Sci.* **1971**, *25*, 598.